ANNALS of Clinical and Translational Neurology
Open Access
ANA American Neurological Association since 1875

RESEARCH ARTICLE

Hyperglycemia- and neuropathy-induced changes in mitochondria within sensory nerves

Hussein S. Hamid[1], Colin M. Mervak[2], Alexandra E. Münch[3], Nicholas J. Robell[2], John M. Hayes[2], Michael T. Porzio[4], J. Robinson Singleton[4], A. Gordon Smith[4], Eva L. Feldman[2] & Stephen I. Lentz[3]

[1]University of Michigan Medical School, University of Michigan, Ann Arbor, Michigan 48109
[2]Department of Neurology, University of Michigan, Ann Arbor, Michigan 48109
[3]Division on Metabolism Endocrinology and Diabetes, Department of Internal Medicine, University of Michigan, Ann Arbor, Michigan 48105
[4]Department of Neurology, University of Utah School of Medicine, Salt Lake City, Utah 84132

Correspondence
Stephen I. Lentz, University of Michigan, 1000 Wall Street, Brehm Tower Room 6245, Ann Arbor, MI. Tel: (734) 647-8233; Fax (734) 232-8175; E-mail: lentzs@med.umich.edu

Funding Information
This work was supported by the National Institutes of Health Grants NS-38849 and DK-076160, the Juvenile Diabetes Research Foundation Center for the Study of Complications in Diabetes, the Program for Neurology Research and Discovery and the A. Alfred Taubman Medical Research Institute at the University of Michigan. This work used the Morphology and Image Analysis Core of the Michigan Diabetes Research and Training Center funded by National Institutes of Health Grant 5P60 DK-20572 from the National Institute of Diabetes and Digestive and Kidney Diseases. H. S. H. received a Program in Neurology Research and Discovery Summer Fellowship funded by the A. Alfred Taubman Medical Institute and a Biomedical and Life Sciences Summer Fellowship through the Undergraduate Research Opportunity Program that was funded, in part, by the Howard Hughes Medical Institute (HHMI). N. J. R., C. M. M. and A. E. M. were supported by HHMI Summer Fellowships.

Received: 20 November 2013; Revised: 19 August 2014; Accepted: 22 August 2014

Annals of Clinical and Translational Neurology **2014; 1(10): 799–812**

doi: 10.1002/acn3.119

Abstract

Objective: This study focused on altered mitochondrial dynamics as a potential mechanism for diabetic peripheral neuropathy (DPN). We employed both an in vitro sensory neuron model and an in situ analysis of human intraepidermal nerve fibers (IENFs) from cutaneous biopsies to measure alterations in the size distribution of mitochondria as a result of hyperglycemia and diabetes, respectively. **Methods**: Neurite- and nerve-specific mitochondrial signals within cultured rodent sensory neurons and human IENFs were measured by employing a three-dimensional visualization and quantification technique. Skin biopsies from distal thigh (DT) and distal leg (DL) were analyzed from three groups of patients; patients with diabetes and no DPN, patients with diabetes and confirmed DPN, and healthy controls. **Results**: This analysis demonstrated an increase in mitochondria distributed within the neurites of cultured sensory neurons exposed to hyperglycemic conditions. Similar changes were observed within IENFs of the DT in DPN patients compared to controls. This change was represented by a significant shift in the size frequency distribution of mitochondria toward larger mitochondria volumes within DT nerves of DPN patients. There was a length-dependent difference in mitochondria within IENFs. Distal leg IENFs from control patients had a significant shift toward larger volumes of mitochondrial signal compared to DT IENFs. **Interpretation**: The results of this study support the hypothesis that altered mitochondrial dynamics may contribute to DPN pathogenesis. Future studies will examine the potential mechanisms that are responsible for mitochondrial changes within IENFs and its effect on DPN pathogenesis.

Introduction

Diabetic peripheral neuropathy (DPN) is a common complication of diabetes occurring in 60–70% of diabetic patients. Distal symmetric sensorimotor polyneuropathy is the most common complication of type 2 diabetes, resulting in length-dependent injury of the longest projecting axons.[1] Possible clinical presentations include asymptomatic neuropathy, painful neuropathy, and painless neuropathy with loss of protective sensation predisposing to foot ulceration and amputation.

Intraepidermal nerve fiber (IENF) density has become an accepted measure of small fiber neuropathies[2–7] and specific guidelines for the use of skin biopsy in the diagnosis of small fiber neuropathy have been established.[8,9] The loss of IENFs is associated with DPN in human diabetic patients[6,10–13] and animal models of diabetes.[14–16] Importantly, there is evidence that therapeutic intervention results in an increase in IENF densities and an improvement in patient assessment of pain in prediabetes associated neuropathy.[17] Despite the usefulness of IENF densities as a measure of neuropathy severity, it is necessary to understand the underlying mechanism responsible for the loss or improvement of IENFs.

Mitochondrial dysfunction has been implicated in a number of neurodegenerative diseases including Alzheimer's disease, amyotrophic lateral sclerosis, Charcot–Marie–Tooth disease, Huntington's disease, hereditary spastic paraparesis, and optic atrophy.[18–22] Notably, a number of studies have demonstrated mitochondrial dysfunction in peripheral neuropathies including chemotherapy- and diabetes-induced neuropathies.[23–28] Studies from our laboratory and others have identified hyperglycemia and diabetes-induced changes in mitochondrial dynamics.[28–33] In particular, changes in mitochondrial fission were observed in the neurites of sensory neurons.[28,30] This study was designed to expand the work on diabetes-induced changes in mitochondrial dynamics. Initial experiments were done in an in vitro sensory neuron model system to examine the effects of hyperglycemia on mitochondria distribution and develop a three-dimensional (3D) analysis technique to measure neurite-specific mitochondria. The novel 3D imaging and analysis technique was then applied to specifically examine mitochondria within IENFs from human cutaneous biopsies in an attempt to translate these in vitro effects to the clinically relevant sensory nerves preferentially lost in DPN.

Materials and Methods

Sensory neuron cultures and image analysis

Timed pregnant rats were purchased from Charles River Laboratories (Wilmington, MA). All rodent care and use was approved and regulated by the Unit for Laboratory Animal Medicine at the University of Michigan. Dissociated dorsal root ganglion (DRG) neurons were isolated from E15 Sprague-Dawley rat embryos following previously published methods.[34] Cultures were maintained at 37°C in a humidified atmosphere containing 5% CO_2. Neurons were used 1–2 days after plating and were treated with or without additional 20 mmol/L glucose for 6 h to promote a hyperglycemic environment.[30,35] Mitochondria were visualized and imaged following previously published methods.[30]

Fluorescent signals in the images were optimized by deconvolution with Volocity software (PerkinElmer, Waltham, MA) using the iterative restoration feature set at 90% confidence level and a period of 10 cycles. Mitochondrial signals from each image were exported from Volocity as OME TIFF files, imported into Imaris, and then saved as Imaris files (IMS).

The built-in surface creator in Imaris was used to create virtual surfaces around neurites with the "background subtraction" method to account for regional changes in fluorescent intensity within the images. A threshold intensity range was chosen specifically for each image in a way that maximized image signal and minimized noise. A subsequent filtering step allowed for the removal of noise from the data set. A filter ranging from 5 to 40 voxels was used for every image depending on the level of noise in that particular image. All remaining objects were surrounded by a 3D virtual surface that was used to extract data. Values were exported from Imaris and into an Excel spreadsheet for all nerve and mitochondrial surfaces to generate a size distribution of mitochondrial signal.

Patient population recruitment

Three groups of patients were studied: seven patients with diabetes and no DPN (DM), seven patients with diabetes and confirmed DPN, and seven age-matched healthy controls (Control). Study subjects were recruited from a large community-based primary care network at the University of Utah Diabetes Center (Salt Lake City, UT). The definition of definite neuropathy was based on the presence of at least three of the following: symptoms of neuropathy, signs based on an abnormal quantitative neurologic examination, abnormality of nerve conducting studies, quantitative sensory testing, quantitative sudomotor axon reflex testing, and skin biopsy with measurement of intraepidermal nerve fiber density (IENFD). Patients included in the analysis accounted for known differences in IENFDs associated with age and gender.[36] Clinical profiles for the patients included in the study are summarized in Table 1. Control subjects were recruited for the study that had no prior history of diabetes or peripheral neuropathy

Table 1. Clinical profile of patient population.

	Age-matched controls	Diabetic patients (DM)	Diabetic peripheral neuropathy patients (DPN)
N	7	7	7
Age (years)	52.8 ± 8.7	53.1 ± 6.3	52.3 ± 9.3
UENS	–	0.6 ± 1.0	9.7 ± 4.3
MDNS	–	0.6 ± 1.0	5.3 ± 3.4
MNSI	–	1.3 ± 1.1	7.1 ± 2.0
HbA1C	–	8.1 ± 1.7	7.2 ± 1.7
Duration (months)			
Diabetes	–	76.9 ± 71.8	69.9 ± 52.4
Neuropathy	–	–	28.7 ± 13.6
IENFD (fibers per mm)			
Distal thigh	7.6 ± 2.0	7.0 ± 2.7	3.0 ± 1.7
Distal leg	5.8 ± 1.2	3.8 ± 2.0	1.0 ± 0.7

Results are means ± SD. UENS, Utah early neuropathy scale; MDNS, Michigan diabetic neuropathy score; MNSI, Michigan neuropathy screening instrument; HbA1C, glycosylated hemoglobin, hemoglobin A1c; IENFD, intraepidermal nerve fiber density.

and were of similar age to the other groups. All subjects signed an informed consent. The University of Utah Institutional Review Board approved the protocol.

Human tissue collection

Each subject underwent a 3-mm skin biopsy from the distal thigh (DT) and distal leg (DL). Samples were subsequently preserved in paraformaldehyde lysine phosphate for 24 h, sectioned at 50 μm, and stored in a cryoprotectant solution (30% glycerin and 30% ethylene glycol in phosphate buffered saline (PBS)).

Fluorescent immunohistochemistry

Tissue sections were pretreated with a block solution of 5% goat serum + 0.3% Triton X-100 (Sigma, St. Louis, MO) detergent solution at room temperature for 1 h with gentle shaking. Sections were incubated with primary antibodies to visualize mitochondria (1:100 mouse anti-pyruvate dehydrogenase (PDH), MitoScience, Eugene, OR) and IENFs (1:1000 polyclonal rabbit anti-PGP-9.5, protein gene product 9.5; AbD Serotek, Raleigh, NC) in an incubation solution (1% goat serum + 0.3% Triton X-100) with gentle shaking at room temperature for 1 h then transferred to 4°C with gentle shaking overnight. Sections were washed three times with the incubation solution and allowed to shake for 1 h after each rinse. Fluorescent secondary antibodies were used to visualize mitochondria (1:1000 goat anti-mouse AlexaFluor-594; Invitrogen, Eugene, OR) and IENFs (1:1000 goat anti-rabbit AlexaFluor-488; Invitrogen) with the same incubation process used for the primary antibodies. Sections were washed twice with 1× PBS for 5 min, followed by two extended washes with shaking at room temperature for 30 min each, and finally transferred to freshly filtered 1× PBS. Skin sections were mounted onto glass slides using Prolong Gold with DAPI (Invitrogen) to fluorescently label nuclei.

Image acquisition and analysis

Slides were masked as to not influence which regions were chosen for imaging. Images were collected with a Leica TCS SP5 confocal microscope system (Leica Microsystems, Inc., Buffalo Grove, IL, USA) using either a 40 × 1.25 numerical aperture (N.A.) or 63 × 1.40 N.A. (the highest magnification and N.A. available on our Leica SP5 confocal system) oil immersion objective on an inverted Leica DMI6000 microscope. Fluorescent signals were sequentially acquired at each focal plane for nuclei (excitation λ = 405 nm, spectral emission filter λ = 420–480 nm), IENFs (excitation λ = 488 nm, spectral emission filter λ = 505–560 nm), and mitochondria (excitation λ = 543 nm, spectral emission filter λ = 606–670 nm). *Z*-series were taken through the extent of the tissue with zoom of 1.7×, frame averaging of 2, step size of 0.17 μm, resolution of 512 × 512 pixels, and 12-bit depth. Four *Z*-series from at least two different tissue sections were taken at 40× from each biopsy site (DT and DL) for every patient. A corresponding 63× image was collected for a subset of the 40× images to directly compare 40× versus 63× as follows: DT: Control n = 2, DM n = 3, and DPN n = 2; and for DL: Control n = 3, DM n = 3, and DPN n = 2. The range and average number of nerves per image were as follows: DT: Control range 4–10, average 5.6, DM range 5–8, average 6.2, and DPN range 4–6, average 4.8; DL: Control range 3–7, average 5.9, DM range 3–10, average 5.9, and DPN range 1–6, average 2.9. *Z*-series that had poor mitochondria labeling were not included in the final

analysis. One-two images were removed from four control patients' thighs, two diabetic thighs, one diabetic leg, one neuropathy thigh, and two neuropathy legs.

As with the image acquisition, images were masked as to not influence the analysis. An imbedded selection and cropping tool within Volocity software was used to isolate the epidermis. The lower edge was cropped precisely at the epidermal–dermal border, where a visible change in the appearance of nerve, nuclei, and mitochondria was observed. The upper edge was cropped to exclude the stratum corneum where the rich mitochondria, nerve, and nuclear stains were no longer present. Image processing and deconvolution was performed using Volocity in the same manner as described above under methods for sensory neuron cultures. These images were exported to Imaris for further analysis.

Imaris classification software made it possible to utilize surfaces created from one fluorescent channel to isolate fluorescent signals in another channel. Thus, the 3D rendering of the nerve signal was used to isolate nerve-specific mitochondrial signal within the nerve surface. The nerve surfaces were created first with the "create surface" tool to make a solid surface of the IENFs from the AlexaFluor-488 fluorescent secondary labeling of the PGP-9.5 identified nerves. The "smoothing" tool was not used and absolute intensity was used to set the threshold for the nerve signal since it was significantly brighter than background fluorescence. Threshold was set to values low enough to accurately mark the nerves. Any small, non-nerve surfaces were filtered out based on size or were edited out from the "Edit" tab by selecting and deleting them. Since we were only interested in the mitochondrial staining within the nerves, we eliminated all of the mitochondrial staining outside the boundary of the nerve surfaces with the use of the Mask Properties options in the Edit tab of the Nerve surface. The "mask all' option was used and the mask channel was set for the AlexaFlour-594 fluorescent signal for mitochondria labeled with the PDH antibody. The "duplicate channel before applying mask" option was selected to preserve the original data, and the mask option was chosen for "Set voxels outside surface to 0." This removed all mitochondrial signals associated with the keratinocytes within the epithelium.[37] The "create surface" tool was then used on the newly created fluorescent channel of the nerve-specific mitochondrial signals that were isolated away from the mitochondrial signal associated with epidermal cells. The "smoothing" tool was not used and the background subtraction option was selected to use local contrast around the mitochondrial signal to render surfaces around the mitochondria. Threshold was set to values low enough to accurately mark mitochondria. Tiny, non-mitochondrial surfaces were filtered out based on size.

Values were exported from Imaris and into an Excel spreadsheet for all nerve and mitochondrial surfaces. Several measurements were collected and calculated for each image: the size distribution of mitochondria in IENFs at the DT and DL regions (placed in bins of increasing size), the size distribution of mitochondria in the keratinocytes of the DT, the number of mitochondria per IENF, and the mitochondrial volume per IENF volume. These values were used to compare between the groups.

Statistical analysis

All values are expressed as means ± SEM. Prism software (version 5.01; GraphPad Software Inc.) was used to determine the overall significance by analysis of variance (ANOVA) and to identify differences between the groups by Tukey's post-hoc tests. Chi-square analysis was performed using GraphPad Software's QuickCalcs (www.graphpad.com). Significance was defined as a $P < 0.05$. Prism was used to plot all graphs.

Results

Visualization and quantification of mitochondria within neurites of cultured sensory neurons

Mitochondria within control DRG neurons and neurons treated with elevated levels of glucose were imaged and processed to create 3D surfaces around the neurite-specific mitochondrial signal to obtain volumetric measurements (Fig. 1A–D). Quantification of mitochondrial volume revealed a significantly greater proportion of mitochondrial signal associated with larger volume ranges after high glucose treatment (Fig. 1E). This 3D analysis technique was used to examine nerve-specific mitochondrial signal in IENFs of human skin biopsies to determine whether the observed hyperglycemic-induced changes in mitochondria within neurites of cultured sensory neurons translated clinically.

Visualization and quantification of mitochondria within human IENFs

Immunofluorescence allowed for simultaneous labeling of multiple signals within the human skin sections that included nerves, mitochondria, and nuclei (Fig. 2A). Signals for nerves and mitochondria were optimized by cropping out regions above and below the epidermis (Fig. 2B). The first step in the analysis was to create 3D surfaces around each nerve (Fig. 2C). The nerve surfaces were then used to crop the nerve-specific fluorescent mitochondrial signal (Fig. 2D). Finally, 3D surfaces were

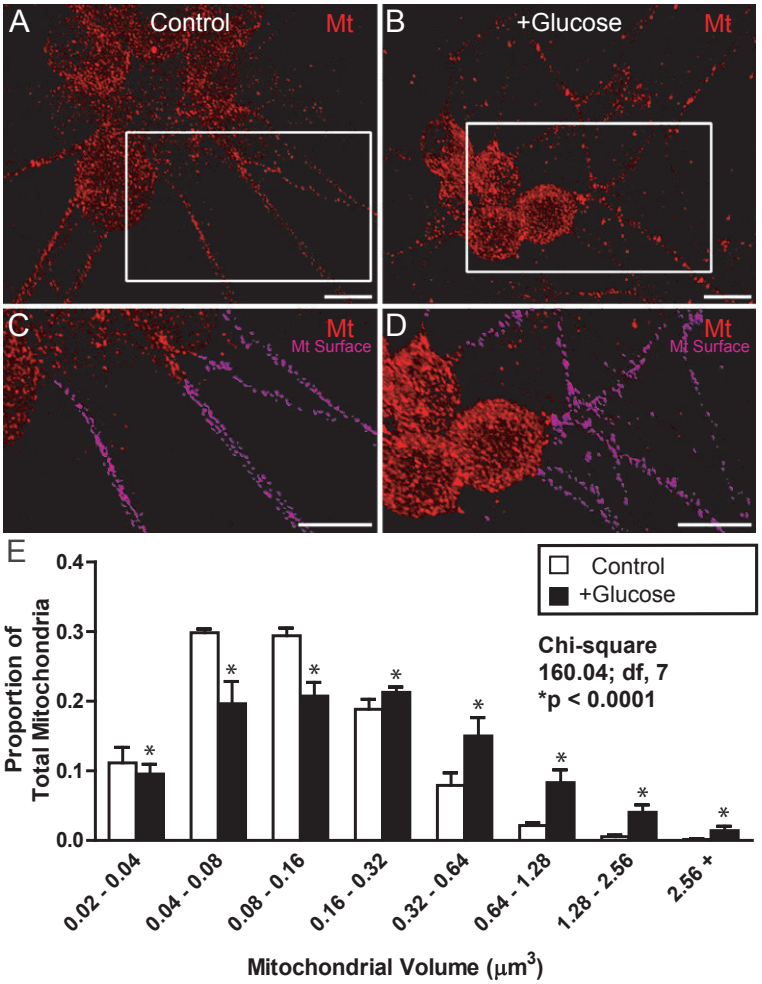

Figure 1. Visualization and summary data for neurite-specific mitochondria within cultured rat dorsal root ganglia neurons grown in control or elevated levels of glucose treatment media for 6 h. (A) Unprocessed image of control neuron illustrates the fluorescent labeling of mitochondria (Mt, red). White box represents the magnified region displayed in (C). (B) Unprocessed image of glucose-treated neuron illustrates the fluorescent labeling of mitochondria (Mt, red). White box represents the magnified region displayed in (D). (C and D) Mitochondrial surface renderings (Mt surface, magenta) were created around neurite-specific mitochondrial signal in control and glucose-treated neurons using Imaris surface creation tool. (E) Data presented as frequency histograms depicting the proportion of mitochondria binned according to size ranges of mitochondrial signal volume (μm^3). Glucose-treated neurons (black bars) had a significantly greater proportion of mitochondrial signal found in larger volume ranges when compared to control neurons (white bars). Values represent means ± SEM, $*P < 0.0001$, versus control group.

created around the nerve-specific mitochondrial signal to obtain volumetric measurements (Fig. 2E).

Mitochondrial distribution in IENFs of the DT

Patient identities were revealed only after all images were processed for nerve and mitochondrial signals. The data were separated into three groups; age-matched controls (Control), diabetic patients (DM), and patients with DPN. Representative 3D images taken with a 40× objective of DT tissue sections demonstrated a visible change in the size distribution of mitochondrial surfaces in the IENFs among the three groups (Fig. 3A–C). Quantification of this change in distribution revealed a significant shift (Chi-square 19.506, df, 7, $P = 0.0067$) in mitochondrial signal in DPN patients resulting in an increased proportion of mitochondrial signal associated with larger volumes (Fig. 3D). Images were taken with a 63× objective of corresponding 40× images to improve the resolution of the mitochondrial signal. Side-by-side comparisons of 40× versus 63× (Fig. 4A and B) demonstrated a slight improvement in resolution of the signals. Rendered surface volumes of the IENF and mitochondrial signals

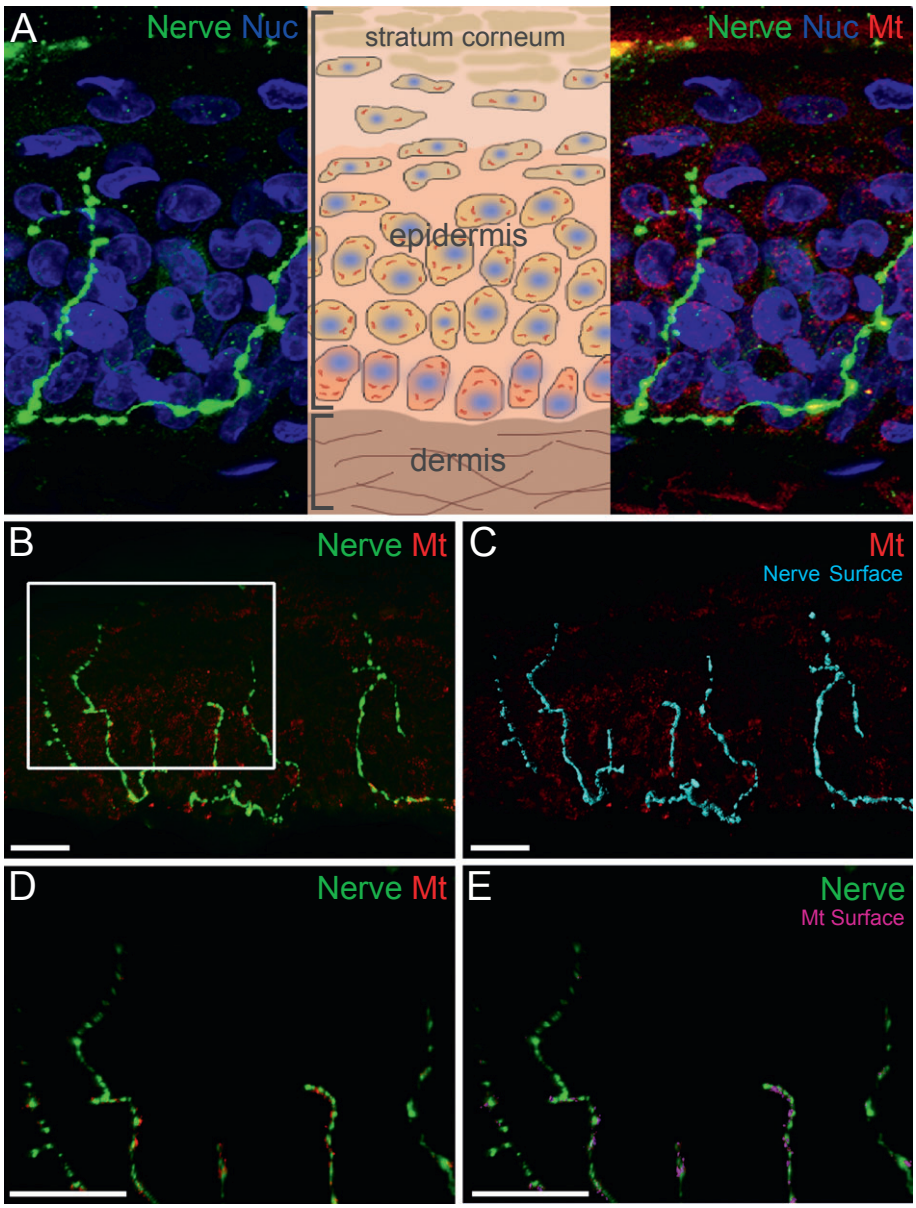

Figure 2. Representative three-dimensional confocal microscopy image of a tissue section from a human epidermal biopsy. (A) Left panel shows nerve (green) and nuclei (Nuc, blue) of keratinocytes within the epidermis. The middle panel is a schematic depicting the corresponding layers of the stratum corneum, epidermis with keratinocytes, and dermis. The right panel includes staining for nerve (green), keratinocyte nuclei (Nuc, blue), and mitochondria (Mt, red). (B) Unprocessed image illustrates the fluorescent labeling of nerve (green) and mitochondria (Mt, red) within the cropped epidermis. White box in (B) represents the magnified region displayed in (D,E). (C) Surface renderings (Nerve Surface, cyan) were created around the nerve signal using the Imaris surface creation tool. (D) Using nerve surfaces, nerve-specific mitochondrial signal (Mt, red) was isolated from the red fluorescent channel. (E) The resulting nerve-specific fluorescent mitochondrial signal was used for further analysis to create surfaces around mitochondria (Mt Surface, magenta). Scale bars = 20 μm.

from the 63× objective were all smaller than their corresponding surfaces from 40×. This was due to the improved numerical aperture of the 63× objective (1.4 vs. 1.25). Despite the smaller volumes, the mitochondrial surfaces appeared to be distributed in similar patterns within the IENFs (Fig. 4C and D). The differences in the frequency distribution of the mitochondrial signals taken with the 63× objective were maintained among the three patient groups (Fig. 4E). In particular, significant shifts in mitochondrial signal size distributions were measured

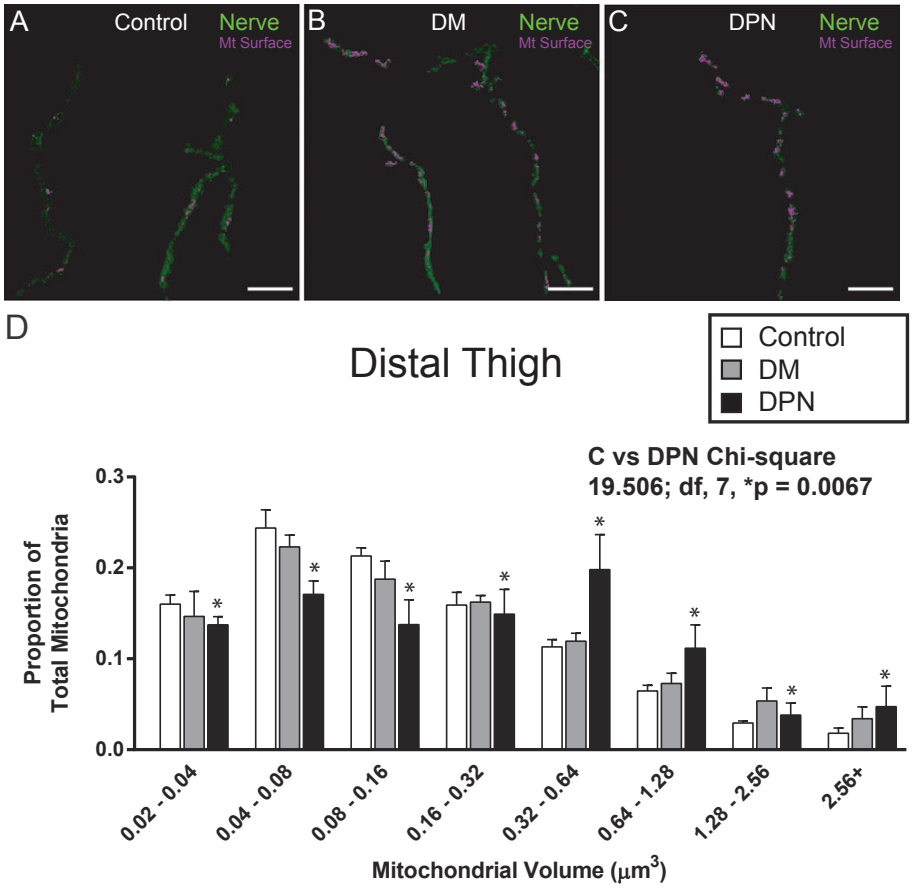

Figure 3. Surface renderings that illustrate the distribution of mitochondria within distal thigh nerves and summary data for mitochondria within intraepidermal nerve fibers of distal thigh from controls, diabetic patients, and patients with diabetic peripheral neuropathy. (A–C) Magnified views of 3D surface renderings that depict nerve-specific mitochondria surfaces (Mt Surface, magenta) overlaid on fluorescent signal for nerves (green). (A) Representative image of age-matched control tissue shows that nerves were fairly abundant in the distal thigh epidermis. Mitochondria were distributed along the nerves. (B) Representative image of distal thigh tissue from a diabetic (DM) patient shows that nerves were also fairly abundant with mitochondria. (C) Distal thigh tissue from patients with diabetic peripheral neuropathy (DPN) had reduced number of nerves innervating the epidermis compared to control and diabetic subjects. These nerves were populated with larger sized mitochondrial signals along the length of the nerves. Scale bars = 10 μm. (D) Data presented as frequency histograms depicting the proportion of nerve-specific mitochondria binned according to mitochondrial volume (μm^3). When all mitochondria were quantified, nerves from diabetic peripheral neuropathy patients (DPN, black bars) exhibited a significant shift toward greater mitochondrial volumes compared to the control group. Values represent means ± SEM.

from both DM (Chi-square 20.89, df, 7, $P = 0.0019$) and DPN patients (Chi-square 48.765, df, 7, $P < 0.0001$), with more mitochondrial signal found within larger volume ranges (Fig. 4E).

Mitochondrial distribution in keratinocytes of the DT

To ensure that the change in mitochondrial size distribution was nerve specific, we also quantified mitochondrial volumes from individual keratinocytes. The same surface creation procedure was used to obtain keratinocyte-specific mitochondrial volumes from the DT samples (Fig. 5A). Unlike in the IENFs, no significant changes in mitochondrial size distribution were observed between controls and DM patients, or between controls and DPN patients (Fig. 5B).

Comparison of mitochondrial distribution in IENFs between DT and DL

Comparison between DT and DL biopsies was performed in order to determine if there were length-dependent differences in mitochondria within IENFs. Mitochondrial volume within IENFs from DL biopsies was calculated for images acquired with the 40× objective (Fig. 6A, C and

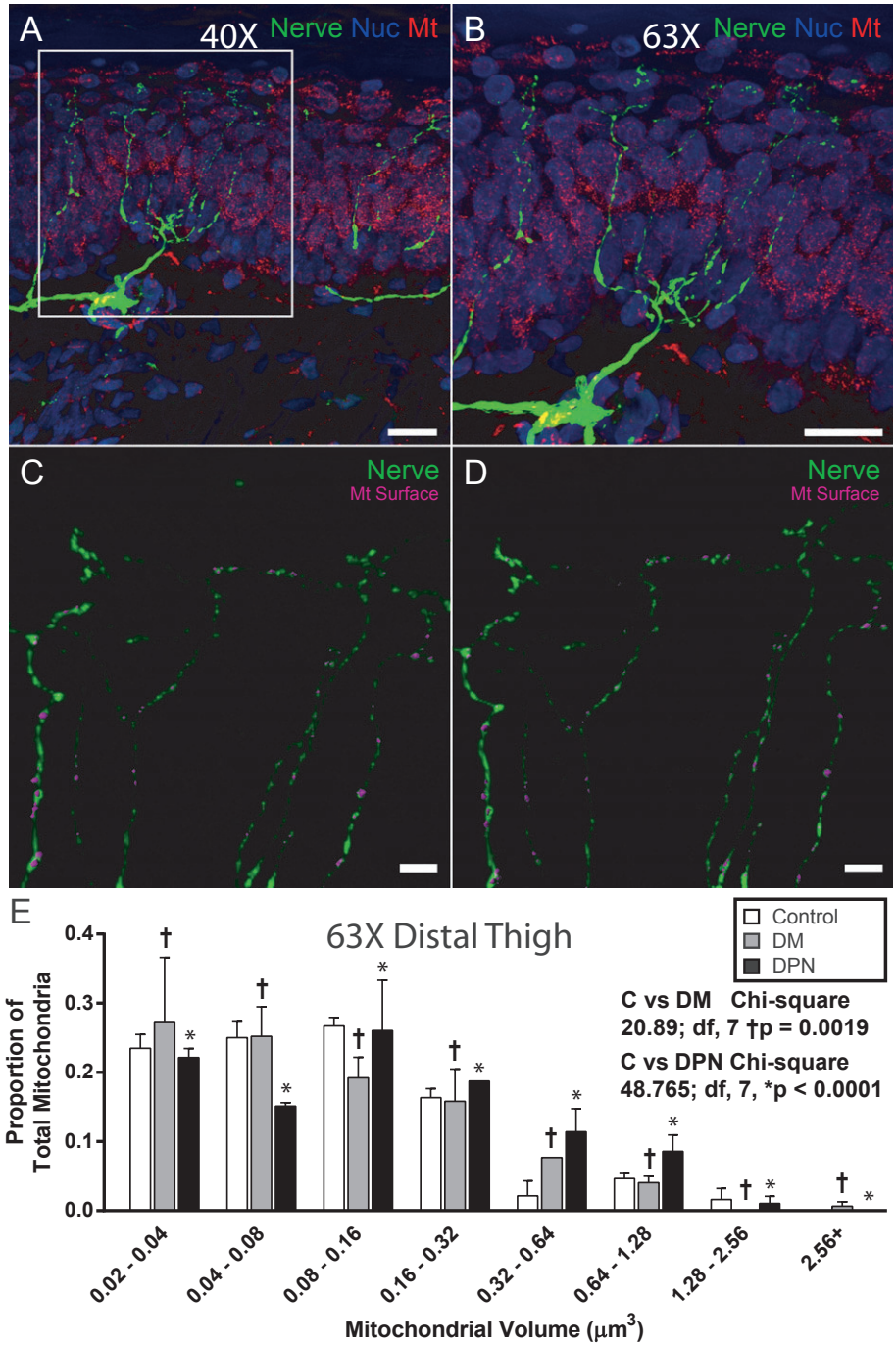

Figure 4. Corresponding three-dimensional confocal microscopy images taken with either a 40× (A and C) or a 63× (B and D) objective of a distal thigh tissue section from a control human epidermal biopsy. (A and B) Panels show fluorescent signals for nerve (green), nuclei (Nuc, blue), and mitochondria (Mt, red). White box in (A) represents the area taken with the 63× objective in B. (C and D) Rendered mitochondrial signals (Mt Surface, magenta) displayed with fluorescent nerve signals (Nerve, green) were distributed in similar patterns between the images taken with the 40× and 63× objectives. Scale bars for A, B = 20 μm and C, D = 5 μm. (E) Data presented as frequency histograms depicting the proportion of nerve-specific mitochondria binned according to mitochondrial volume (μm^3) for the images taken with a 63× objective. When all mitochondria were quantified, nerves from diabetic (DM, gray bars) and diabetic peripheral neuropathy patients (DPN, black bars) exhibited a significant shift toward greater mitochondrial volumes compared to the control group. Values represent means ± SEM.

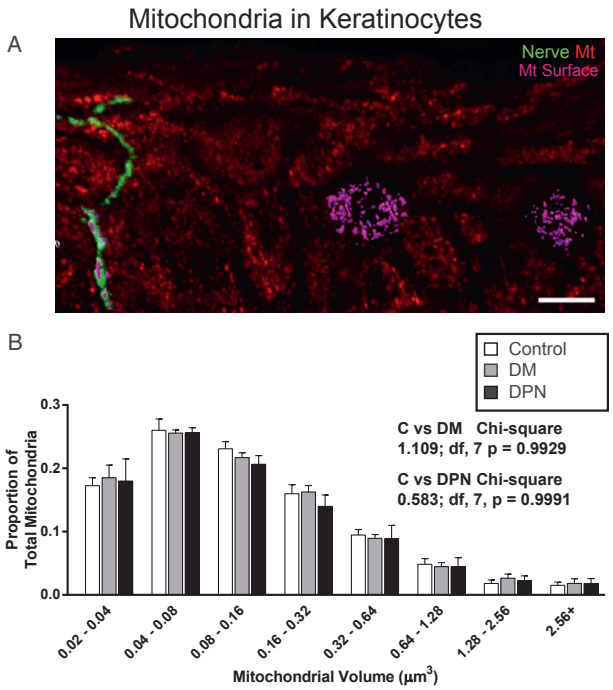

Figure 5. Visualization and summary data of mitochondria within epidermal keratinocytes of distal thigh from controls, diabetic patients, and patients with diabetic peripheral neuropathy. (A) Image from a control patient illustrates the fluorescent labeling of mitochondria (Mt, red) and the mitochondria surfaces created within keratinocytes (Mt Surface, magenta). Image also shows nerve-specific mitochondria surface used in a separate analysis. (B) Data presented as frequency histograms depicting the proportion of keratinocyte-specific mitochondria binned according to appropriate ranges based on mitochondrial volume (μm^3). There was no significant difference in the volume distribution of keratinocyte mitochondria of diabetic (DM, gray bars) nor diabetic peripheral neuropathy (DPN, black bars) patients when compared to controls (white bars). Values represent means ± SEM scale bar 10 μm.

E) similar to the DT biopsies described above. There was a significant (Chi-square 17.519, df, 7, $P = 0.0143$) change in mitochondrial size distribution between the two biopsy sites in the control group with more mitochondrial signal associated with larger volumes in the DL than in the DT (Fig. 6A). The length-dependent shift in mitochondrial size distribution of the control group was not observed in the DL of DM (Fig. 6C) or DPN patients (Fig. 6E). Images taken with the 63× objective were also used to compare nerve-specific mitochondrial signals between the DT and DL (Fig. 6B, D and F). A similar shift toward larger mitochondrial volumes in the DL of control group was measured in the 63× images (Fig. 6B). This shift was also present in the DPN group at 63× (Fig. 6F).

Standard brightfield IENF density counts confirmed a significant decrease in innervation in the DT ($P < 0.001$) as well as the DL ($P < 0.0001$) of DPN patients (Fig. 7A). There was no significant change in the average number of mitochondria per nerve volume across the three patient groups at either the DT or the DL (Fig. 7B). The percent of mitochondrial surface volume per total nerve surface volume was not significantly different among the three groups, although there was a slight increase in the DM and DPN groups compared to controls in both the DT and DL. Higher percentage of mitochondrial volume per nerve volume was measured in the DL compared to the DT (Fig. 7C).

Discussion

Our laboratory and others have focused on alterations in mitochondria as a possible mechanism for neuropathy.[23,27–29,31–33] A recent study examined the role of mitochondria in small fiber neuropathy, focusing on the mitochondria in subepidermal nerve fibers using a 2D analysis method that relied on the colocalization of nerve and mitochondrial signal for quantification.[38] Our study is the first to 3D visualize and quantify changes in mitochondrial distribution within IENFs in man.

Visualization and quantification of mitochondria within neurites of cultured sensory neurons and human IENFs

The combination of fluorescence immunohistochemistry, confocal microscopy, and 3D image analysis allowed for the visualization and measurement of the distribution of mitochondria within neurites and IENFs. The technique was initially developed in an in vitro model system to quantify hyperglycemia-induced changes in the size distribution of mitochondria within neurites of sensory neurons. We then applied this technique to biopsies from diabetic patients and demonstrated that patients with diabetes and DPN have a measureable change in mitochondria distribution within their IENFs compared to age-matched controls.

Proportion of mitochondrial signal associated with larger volumes was increased in DT IENFs of patients with DPN

IENFs in the DT showed a disease-induced change in mitochondrial size distribution. DPN patients had an increased volumetric proportion of mitochondria in their IENFs compared to age-matched control subjects. Interestingly, corresponding higher resolution images (63×, numerical aperture 1.4) of a subset of the data taken with the 40× objective demonstrated a similar shift toward larger mitochondrial volumes in the DPN group as well as

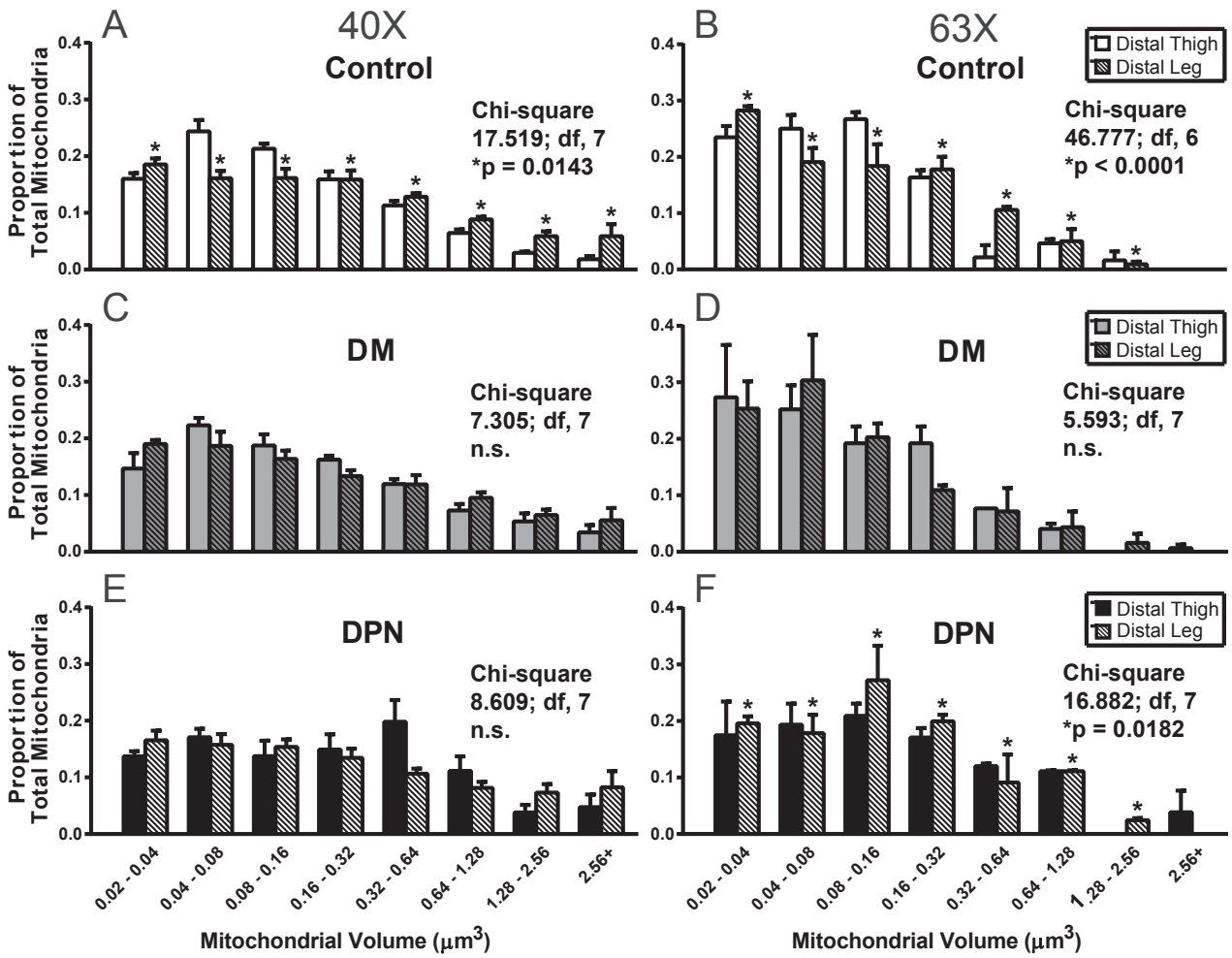

Figure 6. Summary data for mitochondria within intraepidermal nerve fibers of distal thigh compared to distal leg from controls, diabetic patients, and patients with diabetic peripheral neuropathy. Data presented as frequency histograms depicting the proportion of nerve-specific mitochondria binned to mitochondrial volume (μm^3). Analysis of images taken with a 40× objective (A,C and E) were compared to images taken with a 63× objective (B, D, and F). In the control group, distal leg (white hashed bars) samples contained a significantly greater proportion of mitochondria found in larger volume ranges when compared to distal thigh (white solid bars) in both the 40× (A) and 63× images (B). The increased mitochondrial size was not observed in the distal leg (hashed bars) of diabetic patients (DM, gray bars) at either 40× (C) or 63× (D) nor was it shown in the neuropathy (DPN, black hatched bars) patients at 40× (E). A significant shift toward larger mitochondrial volumes was observed in the distal leg (black hashed bars) of DPN patients compared to distal thigh (black bars) when analyzed from images taken with a 63× objective (F). Values represent means ± SEM. n.s., not significant.

the DM group. This suggests that neuropathy could result in increased mitochondria within these nerves.[31] The absence of a similar trend in the keratinocytes from the same samples indicates that this is a nerve-specific phenomenon, and may be associated with neuropathy. A similar increase in mitochondrial signal has been reported after 30-day treatment with mitotoxic linezolid, an antibiotic known to produce sensory peripheral neuropathy.[38]

Changes in mitochondria size distribution in IENFs of the DT might be due to changes in mitochondrial dynamics such as fission, fusion, or trafficking. Our group and others have shown diabetes and neuropathy-induced changes in the fission/fusion machinery of sensory neurons.[28,31,39] It is possible that our observed larger mitochondrial signals could be composed of clusters of smaller, potentially dysfunctional mitochondria that have gone through aberrant fission, or of larger predegenerative, swollen mitochondria.[40–43] In support of this, recent work from our group observed axonal swelling associated with IENFs of patients with diabetic neuropathic pain.[44] It is possible that mitochondrial and axonal swellings are associated with changes in sensory nerve function. Despite

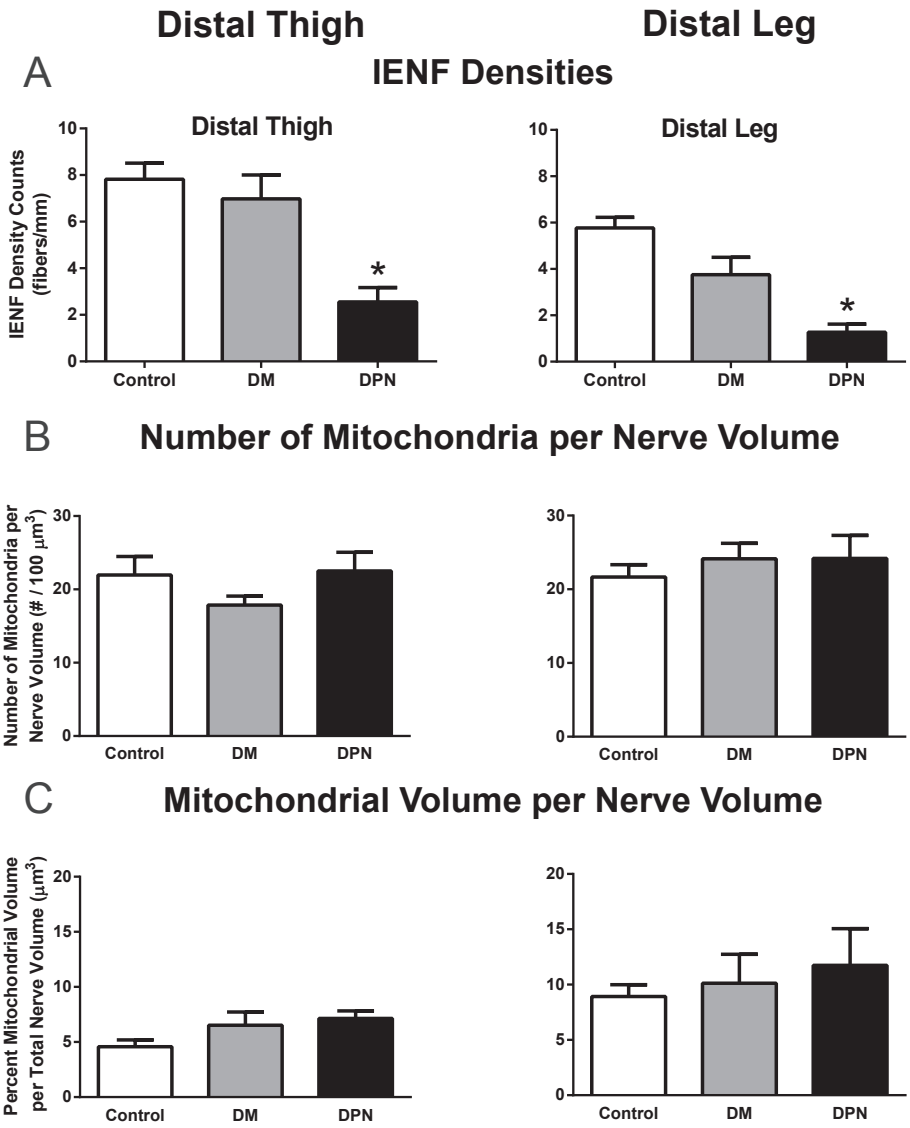

Figure 7. Summary data for intraepidermal nerve fiber density (IENFD), mitochondrial counts, and volumetric proportion of mitochondria in IENFs from the distal thigh and distal leg. (A) IENFD of diabetic patients (DM, gray bar) decreased slightly in the distal leg and significantly with onset of neuropathy (DPN, black bar) in the distal thigh and distal leg. Bars represent means of IENFD (fibers per mm) for each group. (B) There was no significant change in the number of mitochondria per nerve volume across all groups. Bars represent the mean number of mitochondria per IENF volume for each group. (C) Proportion of mitochondrial volume to nerve volume slightly increased with disease progression in both the distal thigh and distal leg. Bars represent means of the percentage of mitochondrial volume (μm^3) per nerve volume (μm^3) for each group. An overall higher percentage of nerve volume containing mitochondria in the distal leg was observed compared to the distal thigh. Values represent means ± SEM.

an attempt to image at a higher resolution with a 63× objective, the mitochondrial signal was not resolved significantly better than with a 40× objective. Further studies at the electron microscopy level will be necessary to resolve these issues.

Another possibility is that larger mitochondrial signals are the result of a disruption in axonal transport, resulting in aggregation or clustering of mitochondria, or failure of larger, swollen mitochondria to transport compared to smaller mitochondria.[45,46] Dysfunction in mitochondrial transport contributes to a variety of neurodegenerative diseases.[47–53] The trafficking and docking of mitochondria are crucial for normal nerve function[54–57] and our findings and others[23,26] suggest a potential role of mitochondrial dynamics in the development or progression of peripheral neuropathy.

Neither diabetes nor DPN significantly altered mitochondria distribution within IENFs of the DL

A well-known characteristic of DPN is the length-dependent loss of sensation.[58] Therefore, mitochondrial signals in IENFs were compared between the DT and DL of all three patient populations. A length-dependent shift toward larger mitochondrial volumes was measured in the DL compared to the DT of the control group. Analysis of the mitochondria from images taken at higher resolution (63× objective) also supported the length-dependent shift in the control group. This length-dependent difference was not observed in the DM and DPN groups in images taken with a 40× objective. However, a shift toward larger mitochondrial volumes was shown in the DL of the DPN group from images taken at the higher resolution. Higher proportions of large mitochondrial volumes in the DL IENFs suggest that mitochondria in these distal nerves are distributed in a similar way to the compromised nerves in the thigh of DPN patients. The shift toward larger mitochondrial volumes distally might support an increased vulnerability of DL IENFs that would make them more susceptible to abnormal mitochondrial functions such as oxidative stress induced by hyperglycemia and diabetes.[28,59]

DT may provide a better region to monitor the effectiveness of therapeutics designed to improve or prevent DPN

The IENFs from the DT showed a differential distribution of mitochondria that is associated with DPN. An increase in mitochondrial aggregates may be a potential mechanism for increased susceptibility for poor nerve fiber function, potential degeneration, or poor regeneration upon injury. In support of this, DPN subjects showed a slower regeneration of DT IENFs than their control counterparts in response to capsaicin-induced denervation.[13] We too have shown that the DT is a better indicator of the beneficial effects of diet and exercise counseling by measuring increased IENF densities after such lifestyle intervention.[13,17] The results of our study suggest that the DT would be a better region to assess the effects of therapeutic interventions designed to lessen or reverse the progression of sensory loss associated with DPN. Future studies might benefit using biopsies from the thigh to study changes in mitochondria distribution in IENFs instead of biopsies from the DL.

In summary, we developed an optical technique to specifically image and quantify nerve mitochondria in the epidermis while excluding mitochondria from other cell sources, such as skin keratinocytes. The results of this study support the hypothesis that altered mitochondrial dynamics may contribute to DPN pathogenesis. These findings provide insight into future research designed to elucidate potential therapeutic interventions directed at regulating mitochondrial networks that may ultimately alleviate or prevent DPN.

Acknowledgments

This work was supported by the National Institutes of Health Grants NS-38849 and DK-076160, the Juvenile Diabetes Research Foundation Center for the Study of Complications in Diabetes, the Program for Neurology Research and Discovery and the A. Alfred Taubman Medical Research Institute at the University of Michigan. This work used the Morphology and Image Analysis Core of the Michigan Diabetes Research and Training Center funded by National Institutes of Health Grant 5P60 DK-20572 from the National Institute of Diabetes and Digestive and Kidney Diseases. H.S.H. received a Program in Neurology Research and Discovery Summer Fellowship funded by the A. Alfred Taubman Medical Institute and a Biomedical and Life Sciences Summer Fellowship through the Undergraduate Research Opportunity Program that was funded, in part, by the Howard Hughes Medical Institute (HHMI). N. J. R., C. M. M., and A. E. M. were supported by HHMI Summer Fellowships.

Conflict of Interest

None declared.

References

1. Little AA, Edwards JL, Feldman EL. Diabetic neuropathies. Pract Neurol 2007;7:82–92.
2. Periquet MI, Novak V, Collins MP, et al. Painful sensory neuropathy: prospective evaluation using skin biopsy. Neurology 1999;53:1641–1647.
3. Lauria G, Lombardi R. Skin biopsy: a new tool for diagnosing peripheral neuropathy. BMJ 2007;334:1159–1162.
4. Holland NR, Crawford TO, Hauer P, et al. Small-fiber sensory neuropathies: clinical course and neuropathology of idiopathic cases. Ann Neurol 1998;44:47–59.
5. Pardo CA, McArthur JC, Griffin JW. HIV neuropathy: insights in the pathology of HIV peripheral nerve disease. J Peripher Nerv Syst 2001;6:21–27.
6. Smith AG, Howard JR, Kroll R, et al. The reliability of skin biopsy with measurement of intraepidermal nerve fiber density. J Neurol Sci 2005;228:65–69.
7. McCarthy BG, Hsieh ST, Stocks A, et al. Cutaneous innervation in sensory neuropathies: evaluation by skin biopsy. Neurology 1995;45:1848–1855.

8. Lauria G, Cornblath DR, Johansson O, et al. EFNS guidelines on the use of skin biopsy in the diagnosis of peripheral neuropathy. Eur J Neurol 2005;12:747–758.
9. Lauria G, Hsieh ST, Johansson O, et al. European Federation of Neurological Societies/Peripheral Nerve Society Guideline on the use of skin biopsy in the diagnosis of small fiber neuropathy. Report of a joint task force of the European Federation of Neurological Societies and the Peripheral Nerve Society. Eur J Neurol 2010;17:903–912, e44–e49.
10. Smith AG, Ramachandran P, Tripp S, Singleton JR. Epidermal nerve innervation in impaired glucose tolerance and diabetes-associated neuropathy. Neurology 2001;57:1701–1704.
11. Sumner CJ, Sheth S, Griffin JW, et al. The spectrum of neuropathy in diabetes and impaired glucose tolerance. Neurology 2003;60:108–111.
12. Kennedy WR, Wendelschafer-Crabb G, Johnson T. Quantitation of epidermal nerves in diabetic neuropathy. Neurology 1996;47:1042–1048.
13. Polydefkis M, Hauer P, Sheth S, et al. The time course of epidermal nerve fibre regeneration: studies in normal controls and in people with diabetes, with and without neuropathy. Brain 2004;127:1606–1615.
14. Sullivan KA, Hayes JM, Wiggin TD, et al. Mouse models of diabetic neuropathy. Neurobiol Dis 2007;28:276–285.
15. Sullivan KA, Lentz SI, Roberts JL Jr, Feldman EL. Criteria for creating and assessing mouse models of diabetic neuropathy. Curr Drug Targets 2008;9:3–13.
16. Lauria G, Lombardi R, Borgna M, et al. Intraepidermal nerve fiber density in rat foot pad: neuropathologic-neurophysiologic correlation. J Peripher Nerv Syst 2005;10:202–208.
17. Smith AG, Russell J, Feldman EL, et al. Lifestyle intervention for pre-diabetic neuropathy. Diabetes Care 2006;29:1294–1299.
18. Sheng ZH, Cai Q. Mitochondrial transport in neurons: impact on synaptic homeostasis and neurodegeneration. Nat Rev Neurosci 2012;13:77–93.
19. Schon EA, Przedborski S. Mitochondria: the next (neurode)generation. Neuron 2011;70:1033–1053.
20. Petrozzi L, Ricci G, Giglioli NJ, et al. Mitochondria and neurodegeneration. Biosci Rep 2007;27:87–104.
21. Maresca A, la Morgia C, Caporali L, et al. The optic nerve: a "mito-window" on mitochondrial neurodegeneration. Mol Cell Neurosci 2013;55:62–76.
22. Su B, Wang X, Zheng L, et al. Abnormal mitochondrial dynamics and neurodegenerative diseases. Biochim Biophys Acta 2010;1802:135–142.
23. Baloh RH. Mitochondrial dynamics and peripheral neuropathy. Neuroscientist 2008;14:12–18.
24. Melli G, Taiana M, Camozzi F, et al. Alpha-lipoic acid prevents mitochondrial damage and neurotoxicity in experimental chemotherapy neuropathy. Exp Neurol 2008;214:276–284.
25. Staff NP, Podratz JL, Grassner L, et al. Bortezomib alters microtubule polymerization and axonal transport in rat dorsal root ganglion neurons. Neurotoxicology 2013;39C:124–131.
26. Chowdhury SK, Smith DR, Fernyhough P. The role of aberrant mitochondrial bioenergetics in diabetic neuropathy. Neurobiol Dis 2013;51:56–65.
27. Zheng H, Xiao WH, Bennett GJ. Functional deficits in peripheral nerve mitochondria in rats with paclitaxel- and oxaliplatin-evoked painful peripheral neuropathy. Exp Neurol 2011;232:154–161.
28. Vincent AM, Edwards JL, McLean LL, et al. Mitochondrial biogenesis and fission in axons in cell culture and animal models of diabetic neuropathy. Acta Neuropathol 2010;120:477–489.
29. Leinninger GM, Edwards JL, Lipshaw MJ, Feldman EL. Mechanisms of disease: mitochondria as new therapeutic targets in diabetic neuropathy. Nat Clin Pract Neurol 2006;2:620–628.
30. Leinninger GM, Backus C, Sastry AM, et al. Mitochondria in DRG neurons undergo hyperglycemic mediated injury through Bim, Bax and the fission protein Drp1. Neurobiol Dis 2006;23:11–22.
31. Edwards JL, Quattrini A, Lentz SI, et al. Diabetes regulates mitochondrial biogenesis and fission in mouse neurons. Diabetologia 2010;53:160–169.
32. Fernyhough P, Roy Chowdhury SK, Schmidt RE. Mitochondrial stress and the pathogenesis of diabetic neuropathy. Expert Rev Endocrinol Metab 2010;5: 39–49.
33. Schmidt RE, Green KG, Snipes LL, Feng D. Neuritic dystrophy and neuronopathy in Akita (Ins2(Akita)) diabetic mouse sympathetic ganglia. Exp Neurol 2009;216:207–218.
34. Leinninger GM, Backus C, Uhler MD, et al. Phosphatidylinositol 3-kinase and Akt effectors mediate insulin-like growth factor-I neuroprotection in dorsal root ganglia neurons. FASEB J 2004;18:1544–1546.
35. Russell JW, Golovoy D, Vincent AM, et al. High glucose-induced oxidative stress and mitochondrial dysfunction in neurons. FASEB J 2002;16:1738–1748.
36. Bakkers M, Merkies IS, Lauria G, et al. Intraepidermal nerve fiber density and its application in sarcoidosis. Neurology 2009;73:1142–1148.
37. Fogarty MJ, Hammond LA, Kanjhan R, et al. A method for the three-dimensional reconstruction of Neurobiotin-filled neurons and the location of their synaptic inputs. Front Neural Circuits 2013;7:1–18.
38. Casanova-Molla J, Morales M, Garrabou G, et al. Mitochondrial loss indicates early axonal damage in small fiber neuropathies. J Peripher Nerv Syst 2012;17:147–157.

39. Courchesne SL, Karch C, Pazyra-Murphy MF, Segal RA. Sensory neuropathy attributable to loss of Bcl-w. J Neurosci 2011;31:1624–1634.
40. Vial JD. The early changes in the axoplasm during wallerian degeneration. J Biophys Biochem Cytol 1958;4:551–555.
41. Mizisin AP, Nelson RW, Sturges BK, et al. Comparable myelinated nerve pathology in feline and human diabetes mellitus. Acta Neuropathol 2007;113:431–442.
42. Park JY, Jang SY, Shin YK, et al. Mitochondrial swelling and microtubule depolymerization are associated with energy depletion in axon degeneration. Neuroscience 2013;238:258–269.
43. Schroder JM, Sommer C. Mitochondrial abnormalities in human sural nerves: fine structural evaluation of cases with mitochondrial myopathy, hereditary and non-hereditary neuropathies, and review of the literature. Acta Neuropathol 1991;82:471–482.
44. Cheng HT, Dauch JR, Porzio MT, et al. Increased axonal regeneration and swellings in intraepidermal nerve fibers characterize painful phenotypes of diabetic neuropathy. J Pain 2013;14:941–947.
45. Court FA, Coleman MP. Mitochondria as a central sensor for axonal degenerative stimuli. Trends Neurosci 2012;35:364–372.
46. Misgeld T, Kerschensteiner M, Bareyre FM, et al. Imaging axonal transport of mitochondria in vivo. Nat Methods 2007;4:559–561.
47. Reynolds IJ, Malaiyandi LM, Coash M, Rintoul GL. Mitochondrial trafficking in neurons: a key variable in neurodegeneration? J Bioenerg Biomembr 2004;36:283–286.
48. Van Laar VS, Berman SB. Mitochondrial dynamics in Parkinson's disease. Exp Neurol 2009;218:247–256.
49. Rui Y, Tiwari P, Xie Z, Zheng JQ. Acute impairment of mitochondrial trafficking by beta-amyloid peptides in hippocampal neurons. J Neurosci 2006;26:10480–10487.
50. Li XJ, Orr AL, Li S. Impaired mitochondrial trafficking in Huntington's disease. Biochim Biophys Acta 2010;1802:62–65.
51. De Vos KJ, Grierson AJ, Ackerley S, Miller CC. Role of axonal transport in neurodegenerative diseases. Annu Rev Neurosci 2008;31:151–173.
52. Chen H, Chan DC. Mitochondrial dynamics–fusion, fission, movement, and mitophagy–in neurodegenerative diseases. Hum Mol Genet 2009;18:R169–R176.
53. Blackstone C, O'Kane CJ, Reid E. Hereditary spastic paraplegias: membrane traffic and the motor pathway. Nat Rev Neurosci 2011;12:31–42.
54. Cai Q, Sheng ZH. Mitochondrial transport and docking in axons. Exp Neurol 2009;218:257–267.
55. Ohno N, Kidd G, Mahad D, et al. Myelination and axonal electrical activity modulate the distribution and motility of mitochondria at CNS nodes of ranvier. J Neurosci 2011;31:7249–7258.
56. Hollenbeck PJ, Saxton WM. The axonal transport of mitochondria. J Cell Sci 2005;118:5411–5419.
57. Kang JS, Tian JH, Pan PY, et al. Docking of axonal mitochondria by syntaphilin controls their mobility and affects short-term facilitation. Cell 2008;132:137–148.
58. Edwards JL, Vincent AM, Cheng HT, Feldman EL. Diabetic neuropathy: mechanisms to management. Pharmacol Ther 2008;120:1–34.
59. Vincent AM, McLean LL, Backus C, Feldman EL. Short-term hyperglycemia produces oxidative damage and apoptosis in neurons. FASEB J 2005;19:638–640.

